

Mechatronic design of a self-balancing three-dimensional inertia wheel pendulum

Johannes Mayr*, Franz Spanlang, Hubert Gatringer

Institute of Robotics, Johannes Kepler University Linz, Altenbergerstrasse 69, Linz, Austria



ARTICLE INFO

Article history:

Received 5 August 2014

Accepted 27 April 2015

Available online 15 July 2015

Keywords:

Inertia wheel pendulum

Optimization

Mechatronics approach

ABSTRACT

In this paper a three-dimensional self-balancing cube is introduced. For stabilization and swing-up, reaction wheels are placed within the cube along with the actuation, electronics and sensors. This allows the cube to swing up from a rest position and to balance around the unstable steady-state positions. We conducted a design assessment to review different design approaches. For the most promising design, we formulated a parameter optimization to calculate the most suitable dimensions for the cube and the inertia elements. These results were used in the mechanical design stage to obtain the optimal design parameters for the cube in an iterative process. To show the effectiveness of the test bench we considered a proportional control law for swing-up and stabilization at the various steady state positions.

© 2015 Elsevier Ltd. All rights reserved.

1. Introduction

Various kinds of underactuated inverted pendulum, such as the Furuta pendulum or the inverted pendulum on a cart, are used as reference models in control theory. Another type of inverted pendulum is the two-dimensional inertia wheel pendulum [1–3], which consists of a physical pendulum and a rotating reaction wheel. We extended this two-dimensional design to a three dimensional (3D) pendulum that has the shape of a cube and is able to balance on its tip and edges. As in the 2D case, the pendulum uses reaction wheels to balance the cube around its equilibrium positions. Analogous to the two dimensional pendulum, the 3D pendulum we propose is hereafter referred to as the *inertia wheel cube* (IWC).

Due to their mechanical structure, the simple but non-linear dynamics of inertia wheel pendulums can be used as a benchmark for non-linear control algorithms. From a pedagogical point of view, inertia wheel pendulums can also serve as simple reference control problems to demonstrate basic ideas of control theory. When balancing on one of its edges, the cube behaves like a 2D inertia wheel. The entire 3D dynamics can be explored while the cube is balancing on its tip.

As already mentioned, inertia wheel pendulums exploit the effects of inertia wheels. Unlike gyroscopic flywheels [4], where a gimbal-suspensioned wheel rotates with a constant speed around

its principal axis of inertia, inertia wheels, also often referred to as reaction wheels, rotate with a variable speed.

Various robotic systems using gyroscopic flywheels to stabilize a vehicle have been presented. While in [5] the stabilization of a bicycle was demonstrated, in [6,7] the authors successfully stabilized a single-wheel robot. Both systems use gimbal motors to deflect the rotating flywheel. Deflecting the rotating flywheel applies a torque around the axis perpendicular to the plane spanned by the axis of deflection and the axis of rotation of the flywheel to the system. By deflecting the flywheel around the axis of gravity, this torque can be used to stabilize the vehicle around the unstable position of rest. Another robotic system consisting of a remote-controlled vehicle and a gyroscopic flywheel was proposed in [8]: the wheel rotates with constant speed and allows driving curves while the car crosses over to the inside of the curve against the centrifugal forces.

Reaction wheels are typically used, for instance, for attitude control in spacecrafts and satellites. Usually, three reaction wheels are mounted along three perpendicular axes. In some cases a fourth inertia wheel is added for redundancy. By varying the speed of the reaction wheels, a reaction torque is applied to the supporting structure. In the case of a free-floating system, such as a satellite or a spacecraft, this reaction torque leads to a rotation of the supporting structure.

Clearly, both kinds of flywheel are able to stabilize an inverted pendulum, but they use different physical effects. To stabilize our 3D inverted pendulum, we employed an approach similar to that used in satellites in our work.

* Corresponding author. Tel.: +43 732 2468 6496.

E-mail addresses: joh.mayr@jku.at (Johannes Mayr), [\(F. Spanlang\)](mailto:franz.spanlang@jku.at), [\(H. Gatringer\)](mailto:hubert.gatringer@jku.at).

Two robots using reaction wheels for stabilization have recently been presented by Murata and can be found on their web page [9]. While Murata Boy is able to ride a bicycle Murata Girl rides on a unicycle. Both robots are stabilized by reaction wheels.

The authors of [10] proposed a testbed for space crafts. The testbed can either be actuated by reaction wheels, fan thrusters or by moving prove masses. The first actuation approach is thus similar to the idea utilized in this paper.

A similar project, named Cubli [11,12], has recently been realized. This system utilizes three inertia wheels mounted on three perpendicular axes. In contrast to the stabilization of satellites, this approach uses active breaks to decelerate the reaction wheels and to swing up the cube to its various steady-state positions. This particular swing-up strategy has the drawback that actively controlling the cube during the brake phase is not possible. As soon as the brakes are released, the motor torques can again be used to control the cube.

In [13] the authors proposed an other three dimensional self balancing cube. Different to our approach this cube does not use flywheels for stabilization. Instead six arms are used to stabilize the cube at its unstable equilibrium positions by rotating the arms and thus shifting the center of mass of the cube.

In this paper, we present a cube that employs a similar actuation system as Cubli, but is able to actively control the swing-up phase, as no breaking system is used. One advantage over the system used in the Cubli test bench is that our system is particularly useful for visualizing gyroscopic effects. One disadvantage compared to Cubli, however, is that it is not capable of swinging up from arbitrary positions to arbitrary unstable positions, as the power-to-weight-ratio of the electric motors is not sufficiently high to generate the reaction torque necessary.

Since our system exhibits non-linear dynamics, it can be used as a test bench for non-linear control algorithms [14,15]. In [16], non-linear control approaches for the inverted pendulum on a cart were introduced. Various non-linear control approaches have been presented that successfully control the attitude of satellites in space. In [3,2,17] various non-linear regulators were applied to the 2D inertia wheel pendulum. A non-linear control approach employing integrator backstepping was used in [18] to control the Cubli. In this paper we are mainly interested in the mechatronics design approach of such a device, but to show the effectiveness of the proposed test bench, we additionally implemented a first approach of a balancing control.

This paper is structured as follows. Before describing the mechatronics design of the IWC in Section 2, we evaluate and compare various design concepts in terms of expected system performance and necessary design efforts. In Section 3, a detailed kinematic and dynamic model is derived for the 3D inverted

pendulum and then used in Section 4 to calculate the optimal size of the cube. In Section 5 the mechanical and electrical design of the cube is described next to a linear control approach used to evaluate the test bench. Sections 6 present simulation and experimental results, respectively, and Section 7 concludes the paper.

2. Design survey

Before we start on the mechatronics design of the IWC, we evaluate and compare various design concepts in terms of system performance and design effort, in order to select a suitable solution to the given task. In total, three different designs are considered, which are summarized in Table 1.

The first design involves a hollow sphere which is supported and driven by three perpendicular omni directional friction wheels that can rotate the sphere in any direction. In this case, the hollow sphere acts as a 3D inertia wheel. The second and third concepts both use conventional cylindrical inertia wheels. While the former employs a separate inertia wheel on every face of the cube, the latter utilizes only three inertia wheels on the faces next to the tip on which the cube is balanced.

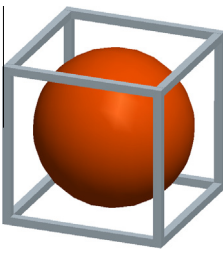
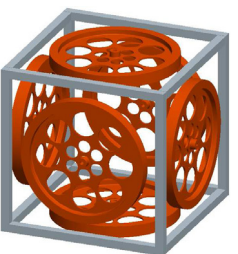
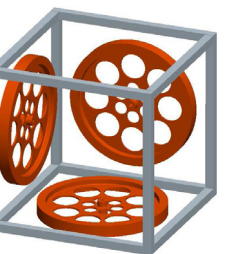
Neglecting the reaction wheel dynamics, the mass of the cube frame and the actuation system, we obtain the simplified model in Fig. 1. This model reduction yields the following equations of motion in the 2D case

$$\tau = (J_0 - J_w)\dot{\varphi} + mga(\varphi), \quad (1)$$

where φ is the position of the cube, τ is the motor torque, J_w is the inertia of the reaction wheel around its axis of rotation, J_0 is the inertia of the whole cube around the edge of the cube, m is the total mass of all reaction wheels, g represents the gravity constant and $a(\varphi)$ is the distance of the center of mass to the edge. Assuming a constant mass m of the reaction wheels, the same side lengths L of the cubes and the same actuation system (represented by similar maximal torques τ_{max}) for all three designs, allows performance comparison on the basis of the simplified 2D model. For $\dot{\varphi}(t) = 0$ the first term on the right hand side of Eq. (1) vanishes and the necessary torque to hold the cube at a certain position is given by $\tau_{hold} = mga(\varphi)$. As m and g are independent of the chosen design variant thus the design which minimizes $a(\varphi)$ is the favorable design. The values for $a(\varphi)$ for $\varphi = 0$ are summarized at the bottom of Table 1.

It can be seen that the last concept with only three cylindrical inertia wheels achieves the highest acceleration to swing up the cube from its resting position. Furthermore, this design variant also seems to involve the least mechanical design effort as mounting and actuation of the inertia elements are straightforward compared to the variant with the hollow sphere.

Table 1
Design variants considered.

Design 1	Design 2	Design 3
		

$$a(0) = \frac{L}{2}$$

$$a(0) = \frac{L}{2}$$

$$a(0) = \frac{L}{3}$$

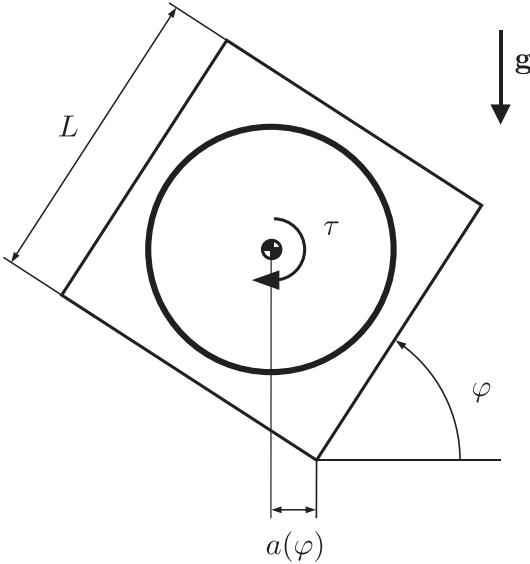


Fig. 1. A simplified model of the IWC for design assessment.

We thus selected the third variant, since it best met the design requirements and promised to be the technically most feasible.

3. Modeling

The design survey in Section 2 shows that for the purpose of a self-balancing cube, a design with three inertia wheels is most favorable. In this section we derive a detailed dynamical model in the form of the equations of motion for this configuration. These equations are used extensively to calculate the design parameters and control laws in the following sections. All variables needed for the description of the kinematic and dynamic model of the cube are summarized in Table 2.

3.1. Kinematic configuration

The kinematic configuration of the IWC is given in Fig. 2. The transformation \mathbf{R}_{IB} from the body-fixed frame Σ_B to the world frame Σ_I can be calculated using the Euler angles \mathbf{q}_1

$$\mathbf{R}_{IB} = \mathbf{R}_B = \mathbf{R}_z(\gamma)\mathbf{R}_y(\beta)\mathbf{R}_x(\alpha), \quad (2)$$

where $\mathbf{R}_i, i \in \{x, y, z\}$ are elementary rotations about the axis i (see [19]). The inverse transformation is given by

Table 2

Variables for equations of motion of the inertia wheel cube.

Variable name	Description
$\mathbf{q} = [\mathbf{q}_1^T \quad \mathbf{q}_2^T]^T$	Generalized coordinates of the whole system
$\mathbf{q}_1 = [\alpha \quad \beta \quad \gamma]^T$	Euler coordinates of the cube frame
$\mathbf{q}_2 = [q_x \quad q_y \quad q_z]^T$	Positions of the inertia wheels
$\dot{\mathbf{s}} = [\mathbf{v}_B^T \quad \dot{\mathbf{q}}_2^T]^T$	Non-holonomic velocities of the whole cube
$\mathbf{B}\omega_B = [\omega_x \quad \omega_y \quad \omega_z]^T$	Angular velocity of the cube frame
$\tau = [\tau_x \quad \tau_y \quad \tau_z]^T$	Torque of inertia wheel drive motors
$m_0 \in \mathbb{R}$	Mass of the total cube
$m_w \in \mathbb{R}$	Mass of an inertia wheel
$\mathbf{r}_C = [s_x \quad s_y \quad s_z]^T$	Position of the center of mass with respect to Σ_B
$\mathbf{J}_0 \in \mathbb{R}^{3 \times 3}$	Inertia tensor of the total cube around the tip with respect to Σ_B
$J_w \in \mathbb{R}$	Moment of inertia of an inertia wheel around the axis of rotation
$L \in \mathbb{R}$	Side length of the cube frame
$g \in \mathbb{R}$	Gravity constant

$$\mathbf{R}_{BI} = \mathbf{R}_{IB}^T = \mathbf{R}_B^T. \quad (3)$$

To calculate the angular velocity vector $\mathbf{B}\omega_B$ of the cube with respect to Σ_B , we can use

$$\mathbf{B}\omega_B = \mathbf{T}(\mathbf{q}_1)\dot{\mathbf{q}}_1 \quad (4)$$

with $\mathbf{T}(\mathbf{q}_1)$ as the transformation matrix that maps Euler velocities to angular velocities.

3.2. Equations of motion

The equations of motion for the given system can easily be derived by dynamics algorithms such as those in [20–22]. Using the Projection Equation from [21] we can calculate the equations of motion for a multi-body system with N bodies

$$\sum_{i=1}^N \left[\left(\frac{\partial \mathbf{r}_C}{\partial \mathbf{s}} \right)^T \left(\frac{\partial \mathbf{B}\omega_B}{\partial \mathbf{s}} \right)^T \right]_i \left[\begin{array}{l} R\dot{\mathbf{p}} + R\tilde{\mathbf{W}}_{IRR}\mathbf{p} - R\mathbf{f}^e \\ R\dot{\mathbf{L}} + R\tilde{\mathbf{O}}_{IRR}\mathbf{L} - R\mathbf{M}^e \end{array} \right]_i = 0 \quad (5)$$

with $R\mathbf{p}_i = m_i \mathbf{v}_{C,i}$ being the vector of linear momentum and $R\mathbf{L}_i = \mathbf{J}_{C,i} R \omega_i$ the vector of angular momentum. The absolute velocity of the center of mass and the angular velocity of the i -th body are given by $R\mathbf{v}_{C,i}$ and $R\omega_i$. External forces acting on the center of mass of the different bodies are considered by $R\mathbf{f}^e$ and $R\mathbf{M}^e$. The $(\tilde{\cdot})$ operator describes the skew symmetric matrix for calculating the cross product ($\tilde{\mathbf{ab}} = \mathbf{a} \times \mathbf{b}$). In (5) one can use a different arbitrary reference frame R for every body, in most cases it is useful to use a body fixed frame as reference frame, as in this case the inertia tensor $R\mathbf{J}_{C,i}$ gets constant w.r.t. time. Evaluating (5) for $N = 4$ bodies (3 inertia wheels + cube frame) finally leads to the equations of motion

$$\mathbf{M}\ddot{\mathbf{s}} + \mathbf{h}(\dot{\mathbf{s}}) + \mathbf{g}(\mathbf{q}_1) = \mathbf{B}\tau \quad (6)$$

with

$$\mathbf{M} = \begin{bmatrix} \mathbf{M}_1 & \mathbf{M}_2 \\ \mathbf{M}_2 & \mathbf{M}_2 \end{bmatrix}, \quad \mathbf{h} = \begin{bmatrix} \mathbf{h}_1 \\ 0 \end{bmatrix}, \quad \mathbf{g} = \begin{bmatrix} \mathbf{g}_1 \\ 0 \end{bmatrix}, \quad \mathbf{B} = \begin{bmatrix} 0 \\ \mathbf{I} \end{bmatrix}$$

where \mathbf{M} describes the mass matrix, \mathbf{h} describes the centrifugal and Coriolis terms, \mathbf{g} are gravity terms, and \mathbf{B} is the input matrix mapping the applied forces and torques in the directions of unconstrained motion.

It can be seen that for the chosen generalized velocities the mass matrix is constant. The entries of the matrices are given by

$$\begin{aligned} \mathbf{M}_1 &= \mathbf{J}_0, \\ \mathbf{M}_2 &= \text{diag}(J_w, J_w, J_w), \\ \mathbf{h}_1 &= \dot{\mathbf{q}}_1 [\mathbf{M}_1 \quad \mathbf{M}_2] \dot{\mathbf{s}}, \\ \mathbf{g}_1 &= m_0 \tilde{\mathbf{r}}_{CB} \mathbf{e}_g g \end{aligned}$$

where $\mathbf{B}\mathbf{e}_g$ is a unit vector in the direction of gravity given in the cube fixed frame.

3.3. Reduction to planar motion

For design parameter optimization, a simplified 2D model is consulted.

Using the principle of virtual work [21], we can map the 3D equations of motion from (6) onto planar forms by a transformation matrix \mathbf{F}

$$\dot{\mathbf{s}} = \frac{\partial \mathbf{s}}{\partial \dot{\mathbf{q}}} \dot{\mathbf{q}} = \mathbf{F} \dot{\mathbf{q}} \quad (7)$$

where $\dot{\mathbf{q}}$ is the vector of reduced describing velocities. As we map the dynamics of the cube onto a 2D motion, the new describing velocities are holonomic. Applying (7) to (6) yields

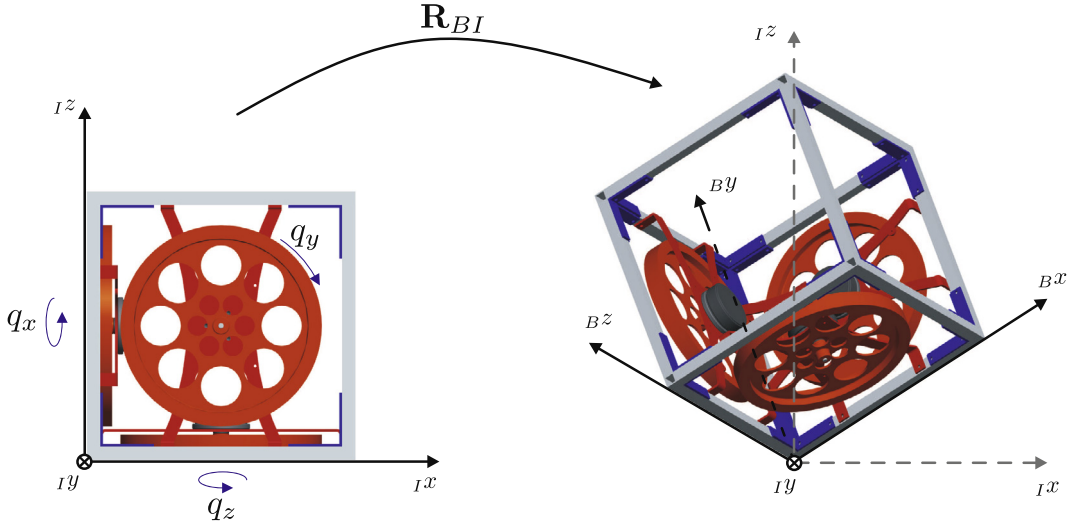


Fig. 2. Kinematic structure of the inertia wheel cube.

$$\bar{\mathbf{M}}\ddot{\mathbf{q}} + \bar{\mathbf{h}}(\dot{\mathbf{q}}) + \bar{\mathbf{g}} = \bar{\tau} \quad (8)$$

with

$$\bar{\mathbf{M}} = \mathbf{F}^T \mathbf{M} \mathbf{F},$$

$$\bar{\mathbf{h}} = \mathbf{F}^T \mathbf{h}(\mathbf{F}\dot{\mathbf{s}}),$$

$$\bar{\mathbf{g}} = \mathbf{F}^T \mathbf{g}(\mathbf{q}_1),$$

$$\bar{\tau} = \mathbf{F}^T \mathbf{B} \tau.$$

The angular velocity of the cube can be expressed as a function of the desired axis of rotation \mathbf{a} and the angular velocity of the cube $\dot{\phi}$ around this axis:

$${}_B\omega_B = \mathbf{a}\dot{\phi}. \quad (9)$$

As the model is reduced to two dimensions, not all inertia wheel velocities can be chosen arbitrarily. Instead the inertia wheel velocities can be expressed as a function of a single velocity denoted by \dot{q}_r

$$\dot{\mathbf{q}}_2 = \mathbf{b}\dot{q}_r, \quad (10)$$

where the matrix \mathbf{b} depends on the rotation axis.

Using (7), (9) and (10) yields for \mathbf{F}

$$\mathbf{F} = \begin{bmatrix} \mathbf{a} & 0 \\ 0 & \mathbf{b} \end{bmatrix} \quad (11)$$

with

$$\dot{\mathbf{q}} = [\dot{\phi} \quad \dot{q}_r]^T. \quad (12)$$

In total, three different reduced models are needed: one for swing-up from a face to an edge (\mathbf{F}_1), one for swing-up from a face to the tip (\mathbf{F}_2), and an other one for the swing-up from an edge to the tip (\mathbf{F}_3). The transformation matrix \mathbf{F}_1 for the face-to-edge swing-up, for example, is given by the rotation axis

$$\mathbf{a}_1^T = [1 \quad 0 \quad 0] \quad (13)$$

and the mapping vector

$$\mathbf{b}_1^T = [1 \quad 0 \quad 0]. \quad (14)$$

One of the three possible representations of the transformation matrix \mathbf{F}_3 for the edge-to-tip swing-up is given by the rotation axis

$$\mathbf{a}_3^T = \left[0 \quad -\frac{1}{\sqrt{2}} \quad \frac{1}{\sqrt{2}} \right] \quad (15)$$

and the mapping vector

$$\mathbf{b}_3^T = [0 \quad -1 \quad 1], \quad (16)$$

which yields an axis of rotation in the y - z plane. In this case, the cube initially balances on the edge that is parallel to the x -axis of the world frame. For the face-to-tip swing-up, the transformation matrix can be chosen as $\mathbf{F}_2 = \mathbf{F}_3$, so that the two models are identical with the exception of the initial angle $\mathbf{q}_1(0)$. In this case, the cube swings up from the face parallel to the y - z plane to the tip.

4. Design dimensioning

With the help of the detailed dynamical model derived in Section 3, optimal design parameters are calculated by defining an objective function representing the optimality of the chosen dimensioning. Finding the optimal design parameters under some given constraints requires solving a classical minimization problem:

$$\min_{\mathbf{p}} J(\mathbf{p}) \quad (17)$$

$$\text{s.t. } \mathbf{g}(\mathbf{p}) = 0 \in \mathbb{R}^p \quad (18)$$

$$\mathbf{h}(\mathbf{p}) \leq 0 \in \mathbb{R}^q \quad (19)$$

(see [23,24] for more details on the formulation of optimization problems). Since the swing-up of the cube can be seen as the most critical part in terms of design parameters, only the different swing-up cases are considered for the optimization.

4.1. Design parameters

Inspecting the equations of motion reveals that numerous different parameters affect the dynamics of the system, most of them depend on other parameters. However, there is a set of parameters \mathbf{p} that is independent. In particular, the side length of the cube L and the mass of the reaction wheels m_w are chosen as independent parameters that allow all inertial parameters and the geometry of the cube to be described. While we fixed the side length at a constant value the mass of the reaction wheels can be varied during the optimization process. The reason for not using the side length as optimization parameter is that for given actuator constraints the side length of the cube will always be at its lower boundary. This can easily be explained by Eq. (1). A smaller side length of the cube

leads to less torque around the axis of rotation as also $a(\phi)$ gets smaller and thus is always favorable to a larger side length.

Further on a desired swing-up trajectory must be defined for $\phi(t)$ because the necessary joint accelerations and torques are a function of ϕ and its derivatives. While an arbitrary function can be used for swing-up, it is recommended to use at least a function that is twice differentiable and has zero acceleration at its boundaries. We use a simple polynomial trajectory

$$\phi(t) = a_0 + a_1 t + a_2 t^2 + a_3 t^3 + a_4 t^4 + a_5 t^5 \quad (20)$$

as swing-up trajectory. The boundary conditions are chosen such that the velocity and the acceleration at the start ($t = 0$) and at the end ($t = t_e$) of the swing-up phase are equal to zero

$$\begin{aligned} \phi(0) &= \phi_0, \\ \phi(t_e) &= \phi_e, \\ \dot{\phi}(0) &= \dot{\phi}(t_e) = 0, \\ \ddot{\phi}(0) &= \ddot{\phi}(t_e) = 0. \end{aligned}$$

The end position ϕ_e is given by the different steady-state positions. The parameterization of the swing-up trajectory adds another two independent variables, given by t_e and ϕ_0 , to the set of independent variables finally leading to

$$\mathbf{p} = [m_w \quad t_e \quad \phi_0]^T. \quad (21)$$

4.2. Dependent parameters

The equations of motion given by (8) contains various parameters which can be expressed as functions of the design parameters given by (21). Since the side length of the cube L and thus the mass

Table 3

Optimal design parameters (m_w, t_e, ϕ_e) for the inertia wheel cube. Shown in brackets are the corresponding values for the real system, where the inertial parameters differ slightly.

m_w in kg	t_e in s	ϕ_0 in rad	ϕ_e in rad
Face to edge	0.09 (-)	1.39 (1.05)	0.42 (0.47)
Face to tip	0.09 (-)	1.28 (1.05)	0.51 (0.59)
Edge to tip	0.09 (-)	1.29 (1.05)	0.17 (0.25)

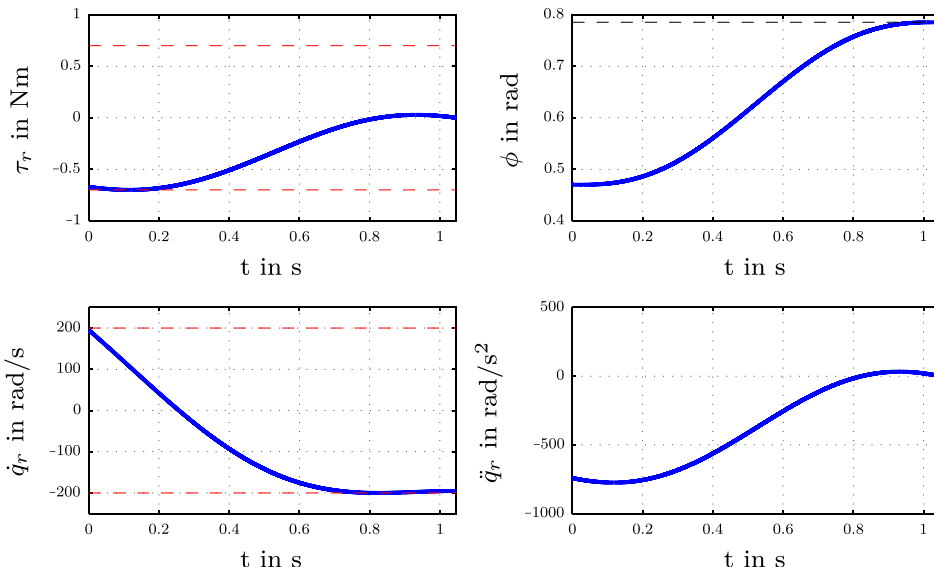


Fig. 3. Trajectory and motor torque necessary for swing-up from a face to an edge. Actuation limits are indicated by red dashed lines. (For interpretation of the references to colour in this figure legend, the reader is referred to the web version of this article.)

of the cube frame m_f is chosen to be constant, the total mass of the cube is given by

$$m_0 = m_f + 3m_w. \quad (22)$$

The mass of the cube frame already contains the parts of the mass of the actuation system fixed to the frame.

To estimate the inertia of the reaction wheels around the rotation axis, the wheels are assumed to be hollow cylinders with width b and inner radius r_2 . The outer radius r_1 is chosen to be a parameter of the cubes side length L with $r_1 = L/2 - b$. The inertia of the reaction wheels is then given by

$$J_w = \frac{r_1^2 + r_2^2}{2} m_w. \quad (23)$$

Further, the mass of the wheel is given by

$$m_w = \rho(r_1^2 - r_2^2)\pi b \quad (24)$$

with ρ as the mass density. The width b of the reaction wheel that leads to the highest inertia is then calculated by rearranging (24) for r_2^2 , substituting the result in (23), and finally setting the derivative of J_w with respect to b equal to zero

$$\frac{\partial J_w}{\partial b} = 0 = 2b + \frac{m^2}{2\rho\pi b^2} - m_w L. \quad (25)$$

As solving (25) for b leads to three different solutions, the physical solution leading to the highest inertia is selected.

4.3. Design constraints

The design constraints are mainly introduced by the actuation of the system and are given by the motor and the motor controller characteristics:

$$|\tau_i| \leq k_m i_{max} \quad (26)$$

$$-\frac{k_m}{R_A} U_{A,max} - \frac{k_m^2}{R_A} \dot{q}_i \leq \tau_i \leq \frac{k_m}{R_A} U_{A,max} - \frac{k_m^2}{R_A} \dot{q}_i \quad (27)$$

$$|\dot{q}_i| \leq \dot{q}_{max}. \quad (28)$$

A description of the constants can be found in Table 4 next to the physical parameters of the chosen motor.

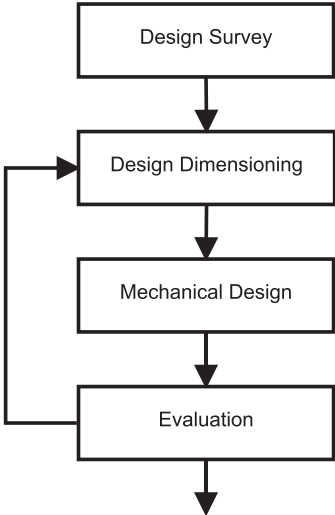


Fig. 4. Iterative design of the inertia wheel cube.

Table 4
Constants of the drive system of the inertia wheel cube.

Variable name	Physical value	Description
i_{max}	25 A	Maximum motor-controller current
\dot{q}_{max}	6110 rpm	No-load speed of the motor
$U_{A,max}$	24 V	Maximum motor and motor-controller voltage
k_m	0.0369 Nm/A	Torque constant of the motor
R_A	0.608 Ω	Phase-to-phase resistance of the motor

Table 5
Specification of our motor controller.

Parameter	Typical rating	Minimum rating	Maximum rating
Logic voltage supply (V)	24	7	26
Logic current (mA)	25	–	50
Motor voltage supply (V)	24	10	30
Motor current (A)	–	–	25
Sensor interface	Quadrature encoder, hall sensors		
Control interface	CAN bus, SPI bus, analog input		

In addition to these constraints, the design parameters must be limited to physically valid ranges

$$0 \leq m_w \quad (29)$$

$$0 \leq t_e \quad (30)$$

$$0 \leq \phi_0. \quad (31)$$

All constraints from (26)–(31) can be summarized in a linear form:

$$\mathbf{h}(\mathbf{p}) = \mathbf{Ap} - \mathbf{b} \leq 0. \quad (32)$$

4.4. Objective function

The objective function

$$J(\mathbf{p}) = \phi_0^2 \quad (33)$$

is used to minimize the initial angle of the cube. Alternatively any other objective function, such as the maximum or average power used during the swing-up process, can be considered.

4.5. Solving the constraint problem

The non-linear parameter optimization (17)–(19) is solved using a gradient-based optimization algorithm, which yields the optimal design parameters for each swing-up case as summarized in Table 3. It can be seen that the resulting parameters are similar for all three cases. Fig. 3 shows by way of example the optimal swing-up trajectory from a face to the edge: all constraints are within the boundaries. Initially, the wheels rotate at a speed of 200 rad/s and decelerate rapidly, causing the cube to swing up due to the resulting reaction torque. Finally, the wheels rotate at a velocity of –200 rad/s.

4.6. Iterative design

In the mechanical design stage described in the next section these optimal parameters are used for dimensioning the cube. As a result of the mechanical design phase new and more accurate information about the inertia parameters of the cube are available. This allows recalculating the optimal design parameters and using them to re-dimension the cube. This iterative design process, summarized in Fig. 4, leads to the optimal design parameters used for the mechanical design. The iteration is terminated if the evaluation shows that the chosen design parameters are sufficiently good for the purpose of a self-balancing inertia wheel cube. In our case we terminate the iterative process at the point where the change in the inertia wheel mass is sufficient small and the gained values lead to realizable cube dimensions. In the next step, the cube prototype is assembled and all inertial parameters are updated to the real ones, since the design dimensioning uses only approximations. Calculating the remaining optimal parameters given by $\bar{\mathbf{p}} = [t_e \ \phi_0]^T$ shows that the minimum starting angles differ slightly from that in the design stage. The new values can be seen in brackets in Table 3 next to the values calculated in the design optimization.

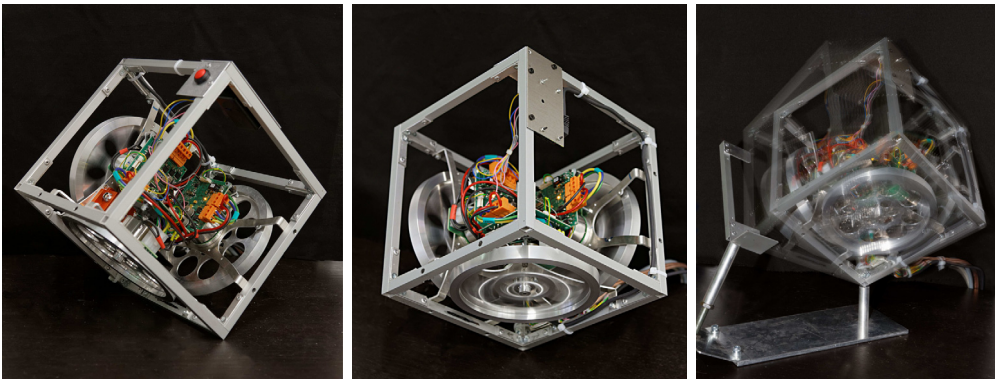


Fig. 5. IWC test bench in different situations: (left) stabilizing on an edge, (middle) stabilizing on the tip, (right) swinging up from its rest position with $\phi_0 \neq 0$.

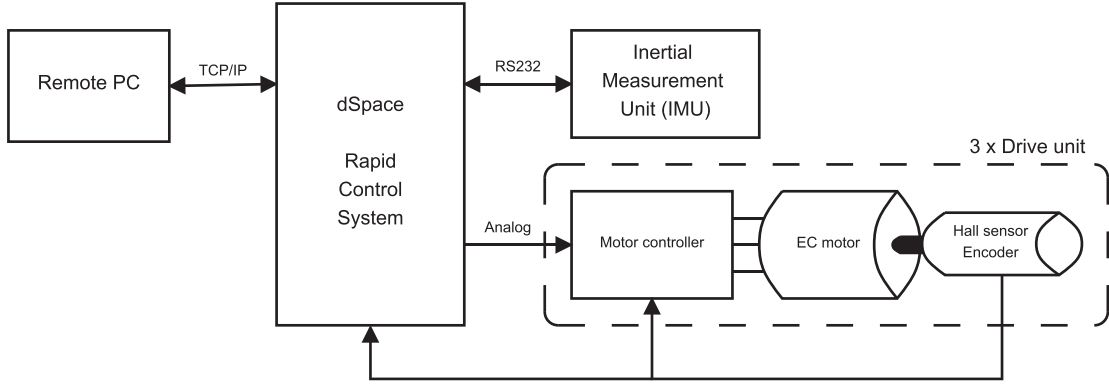


Fig. 6. Control system of the inertia wheel cube.

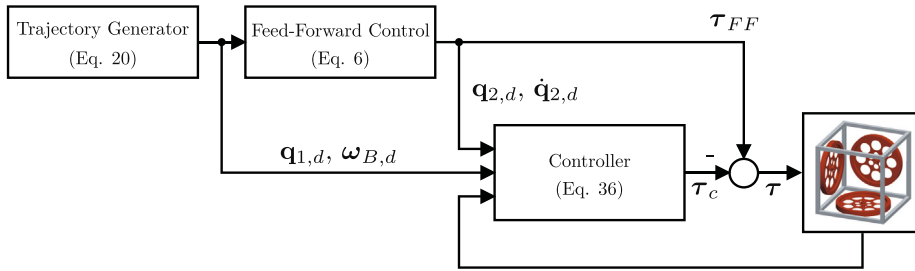


Fig. 7. Schematic of the control law of the inertia wheel cube.

5. Hardware design and implementation

5.1. Mechanical system

The mechanical system consists mainly of the cube frame and mechanical mountings. Since low weight is a key objective for the cube, all structural elements are manufactured from aluminum and glued or riveted together. A picture of the physical system in different situations can be seen in Fig. 5.

5.2. Drive system

Three Maxon EC45-flat PSMS motors are chosen to drive the inertia wheels. The motors with a nominal power of 70 Watts (for more motor parameters see Table 4) are directly mounted on the inertia wheels. To achieve smooth torques at the motor shaft, a field-oriented current control is used. We designed a custom-tailored small and lightweight motor controller for this purpose. In total, three of these motor controllers are mounted inside the cube to maximize system autonomy. Table 5 summarizes the specification of the motor controller.

5.3. Sensor system

For field-oriented control of the motors and for the balance controllers, the motor position is measured using high-accuracy rotary magnetic position sensors directly mounted on the shaft of each motor. A filter is used to approximate the motor velocities.

To measure the current posture and the angular velocity of the cube, a Xsens MTi-30 AHRS [25] inertial measurement unit is mounted on the cube frame. This measurement unit provides drift-free 3D orientation data and high bandwidth gyroscopes suitable for high-precision control of the cube.

5.4. Control hardware

A rapid control prototyping system from dSPACE [26] is used as real-time control system. The control software is developed and debugged with Matlab/Simulink. The dSPACE system allows using the Real Time Workshop (RTW) of Matlab/Simulink to exert control in real-time directly from the Matlab/Simulink simulation. Sensor data are read in via an RS232 interface and the incremental encoder interface of the dSPACE DS1103 system. The analog interface is used to assign the desired motor current to the motor controllers. A remote personal computer is employed to interface with the cube controller. Fig. 6 shows a schematic overview of the control system (see Fig. 7).

5.5. Control implementation

For a first evaluation of the proposed hardware we implemented a control law with feed-forward control based on the equations of motion (6).

The control approach is composed of two parts

$$\tau = \tau_{FF} - \tau_c, \quad (34)$$

where τ_c is the control input, and τ_{FF} corresponds to the feed-forward torque required for the desired orientation. The feed-forward torque can be calculated from (20) using the special structure of (6) and the desired swing-up trajectory (denoted by the index d) as

$$\tau_{FF} = (\mathbf{M}_2 - \mathbf{M}_1)\dot{\omega}_d - \mathbf{h}_1 - \mathbf{g}_1. \quad (35)$$

The control torque is chosen to be

$$\tau_c = \tau_1 + \mathbf{K}_{D1}(\mathbf{B}\omega_{B,d} - \mathbf{B}\omega_B) + \mathbf{K}_{D2}(\dot{\omega}_{2,d} - \dot{\omega}_2) \quad (36)$$

with \mathbf{K}_{D1} and $\mathbf{K}_{D2} \in \mathbb{R}^{3 \times 3}$ being the positive definite diagonal damping matrices for the cubes posture and the inertia wheels position.

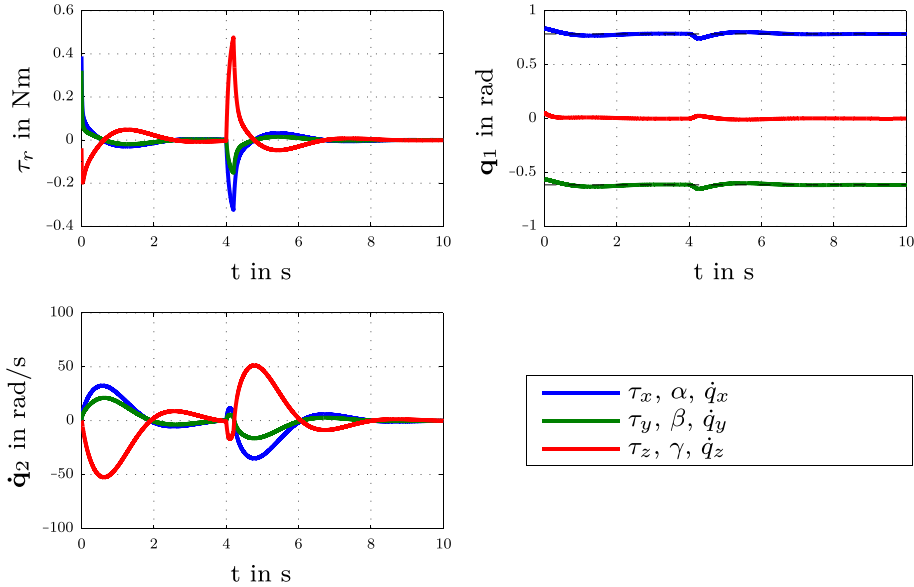


Fig. 8. Simulations with the cube balancing on the tip. At $t = 0$ s, the simulation starts with a small deflection from the upper equilibrium. At $t = 4$ s, a disturbance is applied to the cube.

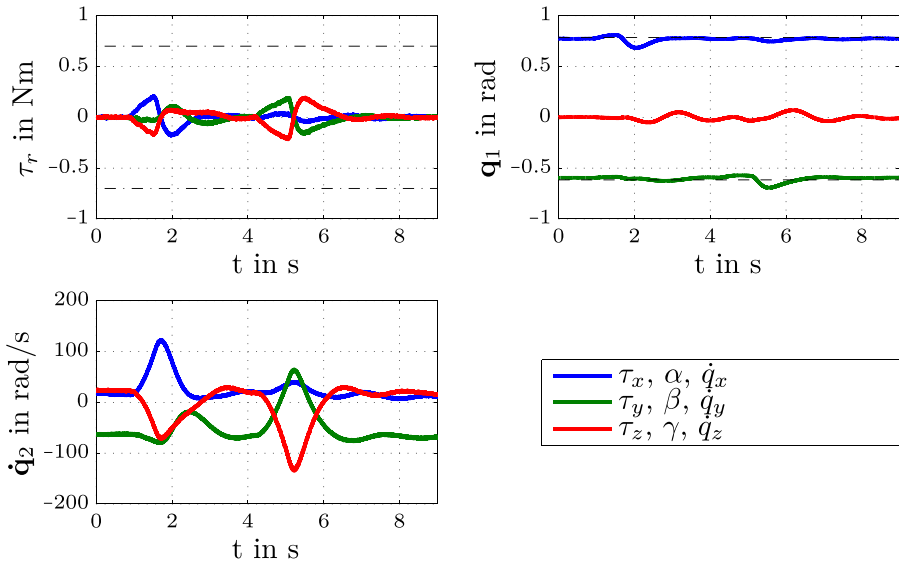


Fig. 9. Experiment with the cube balancing on the tip while disturbances are applied at around $t = 1$ s and $t = 4.2$ s.

The control input τ_1 , which compensates for orientation perturbations, uses an angle-/axis-based representation to (i) avoid singularities that would be introduced by an Euler angle representation, and (ii) realize a rotational stiffness that is independent of the desired posture of the cube (see [27]). The misalignment of the cube is given by its measured orientation \mathbf{R}_B and the desired posture $\mathbf{R}_{B,d}$

$$\mathbf{R}_e = \mathbf{R}_{B,d}^T \mathbf{R}_B. \quad (37)$$

From (37), the axis of rotation \mathbf{u} and the corresponding rotation angle θ can be used to calculate a torque proportional to the orientation error

$$\tau_1 = \mathbf{K}_0 \sin(\theta) \mathbf{u}, \quad (38)$$

where $\mathbf{K}_0 \in \mathbb{R}^{3 \times 3}$ is a positive definite diagonal matrix.

5.5.1. Control dimension reduction

The unstable equilibrium of the cube balancing on the tip allows free rotation about the gravity axis. Thus, arbitrary positions

around this axis can be realized by setting the control torque around this axis to zero. This yields a cube that can be rotated freely around the gravity axis by an external torque applied to this axis. Such control behavior can be realized simply by mapping the control torques onto a world fixed frame where the z-axis is aligned with the gravity axis. The corresponding entry is then set to zero by using a selection matrix \mathbf{S} . The resulting torque vector is rotated back into the body fixed frame by

$$\tau_1^\perp = \mathbf{R}_B^T \mathbf{S} \mathbf{R}_B \tau_1 \quad (39)$$

with

$$\mathbf{S} = \begin{bmatrix} 1 & 0 & 0 \\ 0 & 1 & 0 \\ 0 & 0 & 0 \end{bmatrix}.$$

In (36), τ_1^\perp is now used instead of τ_1 .

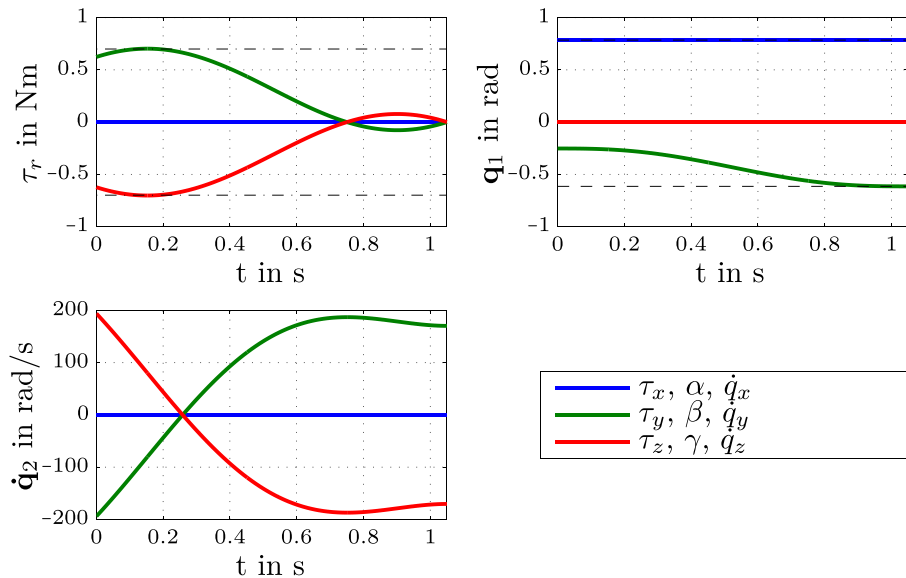


Fig. 10. Simulations for the cube swinging up from an edge to the tip.

5.5.2. Stability analysis

To prove the stability of the controller from (34) around the unstable equilibrium position, the eigenvalues of the linearized closed-loop system are calculated. Using the nonlinear system dynamics from (6), the dynamics can be transformed into a state space representation

$$\dot{\mathbf{x}} = \begin{bmatrix} \dot{\mathbf{q}}_1 \\ \dot{\mathbf{s}} \end{bmatrix} = \mathbf{f}_1(\mathbf{x}) + \mathbf{h}(\mathbf{x}, \boldsymbol{\tau}) = \begin{bmatrix} \mathbf{J}(\mathbf{q}_1)\dot{\mathbf{s}} \\ \mathbf{M}^{-1}(\mathbf{B}\boldsymbol{\tau} - \mathbf{h}(\dot{\mathbf{s}}) - \mathbf{g}(\mathbf{q}_1)) \end{bmatrix} \quad (40)$$

with

$$\mathbf{J} = [\mathbf{T}(\mathbf{q}_1)^{-1} \quad \mathbf{0}].$$

Substituting the control input (34) and (36) into (40) yields

$$\dot{\mathbf{x}} = \mathbf{f}_2(\mathbf{x}). \quad (41)$$

Linearizing (41) about the unstable equilibrium results in

$$\dot{\mathbf{x}} = \mathbf{A}\mathbf{x} \quad (42)$$

with the dynamic matrix \mathbf{A} . A detailed analysis of the eigenvalues of the dynamic matrix shows that for positive definite gains \mathbf{K}_{D1} , \mathbf{K}_{D2} and \mathbf{K}_0 the real parts of the eigenvalues are negative. Therefore the linearized system is stable around the upper equilibrium of the cube.

The linearized system also remains stable (with one zero eigenvalue corresponding to the free rotation around the gravity axis) when the rotation about the gravity axis is no longer controlled ((39) is then used instead of (36)).

This stability analyses is only valid for an area around the equilibrium state, but as the scope of this paper is focused on the mechatronics design approach we are not going into more detail and abstain on further stability analyses.

6. Results

To evaluate the test bench described in above sections, we simulated various conditions like swing-up or balancing using Matlab/Simulink. For all simulations the inertial parameters of the real system (all masses were measured, all distances and inertias were taken from drawings) were used: $m_0 = 1.94$ kg, $m_w = 0.21$ kg, $s_x = s_y = s_z = 0.08$ m, $J_w = 0.905 \cdot 10^{-3}$ kg m², $J_0^{ii} = 0.04$ kg m²,

$J_0^{ij} = -0.012$ kg m². The parameters of the actuation system were chosen according to Table 4. Controller gains were chosen to be $\mathbf{K}_0 = \text{diag}(4, 4, 4)$, $\mathbf{K}_{D1} = \text{diag}(0.5, 0.5, 0.5)$ and $\mathbf{K}_{D2} = \text{diag}(0.001, 0.001, 0.001)$.

6.1. Balancing in the unstable tip position

First, the cube was balanced on its tip using the controller from (34). Simulation results are shown in Fig. 8. Even if the initial position of the cube is incorrect, the controller is able to stabilize the cube into the steady-state position while not violating the actuator constraints. In this simulations at time $t = 4$ s, a disturbance was applied to the cube. It can be seen that after a deflection from the steady-state position, the controller was able to stabilize the cube into the upper equilibrium position.

Analogous to the simulations, an experiment with the physical cube balancing on its tip was conducted. The results are shown in Fig. 9. Clearly, the controller was able to compensate for different disturbances applied to the cube. Looking at the wheel's speed it can be seen that the desired equilibrium position does not completely coincide with the actual one. The fault in the equilibrium position is compensated by a non-zero wheel velocity as the posture controller (given by (38)) accelerates the wheels while the wheel velocity damping (given by \mathbf{K}_{D2} in (36)) slows down the wheels. Eventually a balance between orientation deflection and wheel velocity is reached (see \dot{q}_y in Fig. 9).

6.2. Swinging up to the unstable tip position

Next, a simulation with the cube swinging up from its edge aligned with the x-axis to the tip was carried out. The starting angle was chosen according to Table 3. In Fig. 10 can be seen that the cube swings up to the steady-state position and then balances on the tip. As the starting angle was chosen so that all constraints given by (26)–(31) were satisfied, the joint torques and velocities were within the boundaries.

A second experiment was conducted where the cube swung up from the edge aligned with the z-axis to the tip. The results in Fig. 11 show that the controller was able to swing up the cube from its edge successfully. Due to the cabling that connects the cube with the external control system an unknown disturbance torque is

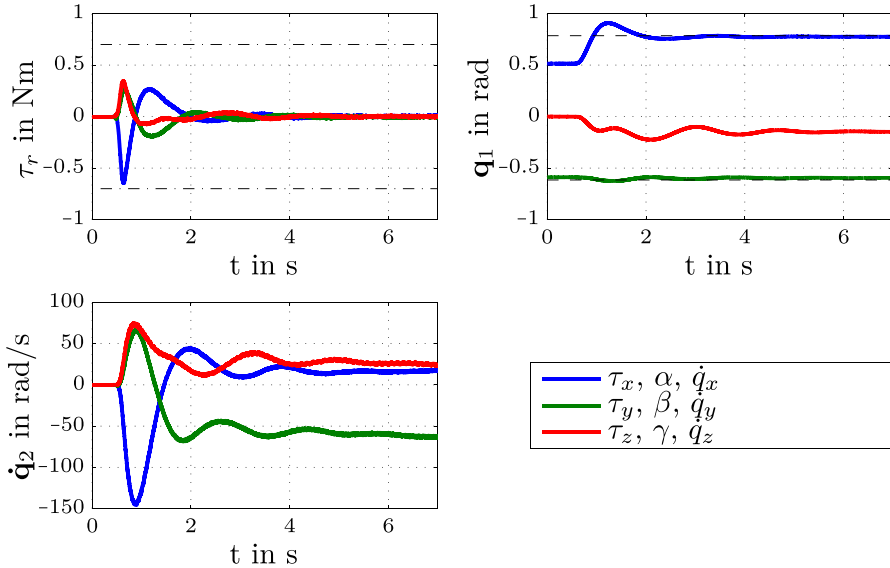


Fig. 11. Experiment with the cube swinging up from the edge to the tip.

applied to the robot and leads e.g. to a rotation around the inertial z -axis (can be seen by the trend of γ in Fig. 11). Additionally in this experiment we did not decelerate the wheels from an initial wheel velocity, instead we started with zero velocity of the inertia wheels.

7. Conclusion

We have presented the development and control of a self-balancing three-dimensional inertia wheel pendulum in the shape of a cube. The cube is used as a test bench for non-linear control and as a demonstration platform for students. A design assessment identified the most suitable and technically feasible design of the cube. Stabilization of the cube is realized by three perpendicular inertia wheels driven by brushless DC motors. For swing-up and stabilization in the unstable steady-state positions, a control law was introduced and successfully tested in simulations and on the real system. In contrast to similar projects, like the Cubli [11,12], the proposed approach actively controls the deceleration of the inertia wheels and thus gives full control of the whole swing-up phase. Further on the geometry of the proposed system is optimized for the use case. In the future an integrated control system will replace the external one, allowing the cube to be operated fully autonomously without any external cabling.

Acknowledgments

This work was supported by the Austrian COMET-K2 program of the Linz Center of Mechatronics (LCM), and was funded by the Austrian federal government and the federal state of Upper Austria.

Appendix A. Supplementary material

Supplementary data associated with this article can be found, in the online version, at <http://dx.doi.org/10.1016/j.mechatronics.2015.04.019>.

References

- [1] Spong MW, Corke P, Lozano R. Nonlinear control of the inertia wheel pendulum. *Automatica* 1999;37:1845–51.
- [2] Olfati-Saber R. Global stabilization of a flat underactuated system: the inertia wheel pendulum. In: Proceedings of the 40th IEEE conference on decision and control; 2001. p. 3764–5.
- [3] Ortega R, Spong MW, Goméz-Estern F, Blankenstein G. Stabilization of a class of underactuated mechanical systems via interconnection and damping assignment. *IEEE Trans Autom Control* 2002;47:1218–33.
- [4] Magnus K. Gyroscopes, theory and applications. Berlin: Springer; 1971 [in German].
- [5] Beznos AV, Formal'sky A, Gurfinkel EV, Jicharev DN, Lensky AV, Savitsky KV, et al. Control of autonomous motion of two-wheel bicycle with gyroscopic stabilisation. In: Proceedings of the IEEE international conference on robotics and automation, vol. 3; 1998. p. 2670–5.
- [6] Yangcheng Xu YO. Control of single wheel robots. Berlin: Springer Verlag; 2005.
- [7] Park J, Jung S. Development and control of a single-wheel robot: practical mechatronics approach. *Mechatronics* 2013;23(6):594–606.
- [8] Huber J, Clauberg R, Ulbrich H. Herbie: demonstration of gyroscopic effects by means of a rc vehicle. In: Proceedings of the 8th international conference on multibody systems, nonlinear dynamics and control; 2011.
- [9] Murata. Murata robots; 2014. <<http://www.murata.com/en-us/about/mboymgirl>>.
- [10] Bernstein D, McClamroch N, Bloch A. Development of air spindle and triaxial air bearing testbeds for spacecraft dynamics and control experiments. In: Proceedings of the American control conference, vol. 5; 2001. p. 3967–72.
- [11] Gajamohan M, Merz M, Thommen I, D'Andrea R. The cubli: a cube that can jump up and balance. In: Proceedings of the international conference on intelligent robots and systems; 2012. p. 3722–7.
- [12] Gajamohan M, Muehlebach M, Widmer T, D'Andrea R. The cubli: a reaction wheel based 3d inverted pendulum. In: Proceedings of the European control conference; 2013. p. 268–74.
- [13] Trimpf S, D'Andrea R. The balancing cube: a dynamic sculpture as test bed for distributed estimation and control. *IEEE Control Syst Mag* 2012;32(6):48–75.
- [14] Isidori A. Nonlinear control systems. Springer; 1985.
- [15] Khalil HK. Nonlinear systems. 3rd ed. New Jersey: Prentice Hall; 2002.
- [16] Gomez-Estern F, Ortega R, Rubio F, Aracil J. Stabilization of a class of underactuated mechanical systems via total energy shaping. In: Proceedings of the 40th IEEE conference on decision and control; 2001. p. 1137–43.
- [17] Santibanez V, Kelly R, Sandoval J. Control of the inertia wheel pendulum by bounded torques. In: Proceedings of the 44th IEEE conference on decision and control and the european control conference; 2005. p. 8266–70.
- [18] Muehlebach M, Gajamohan M, D'Andrea R. Nonlinear analysis and control of a reaction wheel-based 3d inverted pendulum. In: Proceedings of the conference on decision and control; 2013.
- [19] Craig JJ. Introduction to robotics: mechanics and control. 3rd ed. Prentice Hall; 2004.
- [20] Khalil W, Dombre E. Modeling, identification and control of robots. London: Kogan Page Science; 2004.
- [21] Bremer H. Elastic multibody dynamics: a direct ritz approach. Heidelberg: Springer Verlag; 2008.
- [22] Gatringer H, Bremer H, Kastner M. Efficient dynamic modeling for rigid multi-body systems with contact and impact. *Acta Mech* 2011;219:111–28.
- [23] Diehl M. Lecture notes on numerical optimal control. K.U. Leuven; 2011.
- [24] Nocedal J, Wright SJ. Numerical optimization. New York: Springer; 2006.
- [25] Xsens. 3d motion tracking; 2014. <<http://www.xsens.com>>.
- [26] dSPACE. Digital signal processing and control engineering; 2014. <<http://www.dspspace.com>>.
- [27] Caccavale F, Natale C, Siciliano B, Villani L. Six-dof impedance control based on angle/axis representations. *IEEE Trans Robot Autom* 1999;15:289–300.